Metal Deposition

DOI: 10.1002/ange.201405274

Sorption-Determined Deposition of Platinum on Well-Defined Platelike WO_3**

*Kasper Wenderich, Aram Klaassen, Igor Siretanu, Frieder Mugele, and Guido Mul**

Abstract: *The photodeposition of Pt nanoparticles from $[PtCl_6]^{2-}$ on platelike WO_3 crystals occurs preferentially on the small, subordinate facets. Rather than the often-used explanation of preferred light-induced charge migration, we propose that this phenomenon is due to differences in the intrinsic surface charges of WO_3 facets exposed to water; thus, the dark sorption of $[PtCl_6]^{2-}$ on positively charged facets/edges is preferred. This conclusion is based on 1) (dark) impregnation studies, which showed Pt deposition to also be facet-specific, and 2) aqueous-phase AFM studies, which suggest intrinsic surface charges to be in agreement with sorption-based Pt distributions.*

In recent years, the photodeposition of nanoparticulate metals and metal oxides on various semiconductor crystals has been used frequently to optimize photocatalytic performance. Interestingly, various studies have demonstrated a specific spatial distribution of these nanoparticles on photocatalytically active crystals. For example, Ohno et al. observed metal deposition preferentially on the {110} facet and the {011} facet of rutile and anatase phases, respectively, whereas (lead) oxide deposition on the {011} facet and the {001} facet appeared to be preferred.[1] Miseki et al. showed the accumulation of Au or Ni on very different facets of $BaLa_4Ti_4O_{15}$ as compared to PbO_2.[2] Furthermore, Iizuka et al. observed the preferred positioning of Ag on the same $BaLa_4Ti_4O_{15}$ photocatalyst.[3] Finally, Li et al. convincingly demonstrated the presence of spatial nanoparticle distributions after the photodeposition of Pt on $BiVO_4$.[4] Generally, two reasons for preferred photodeposition have been proposed. Ohno et al., Iizuka et al., and Li et al. advocate a theory according to which illumination results in the preferred migration of holes and electrons to specific crystal facets, thus resulting in locations where reduction reactions (and metal deposition) preferentially occur, and other locations where oxidation reactions are dominant (and result in oxide deposition).[1] Alternatively, Miseki et al. ascribe the structure-directed deposition of Au, Ni, and PbO_2 on $BaLa_4Ti_4O_{15}$ to preferred sorption phenomena, thus implying that differences in the intrinsic surface charge of facets should be present under conditions of photodeposition.[2]

Tungsten trioxide (WO_3) is one of the most studied semiconductor materials in photocatalysis.[5] WO_3 is chemically stable under acidic conditions, is nontoxic, and has a relatively narrow bandgap (ranging from 2.4 to 2.8 eV), thus enabling the absorption of visible light in the blue range: a significant part of the solar spectrum.[5,6] WO_3 has been used successfully in Z-scheme configurations for overall water splitting.[7] Additionally, WO_3 loaded with Pt nanoparticles shows significant photocatalytic activity in wastewater treatment.[6a,8] Often photodeposition is used to prepare platinum-loaded WO_3.[8c,d,9] Although the photocatalytic behavior of platinum-modified WO_3 has been reported frequently, to the best of our knowledge no detailed reports have been published on a preferential location of deposited Pt on WO_3 crystals or the mechanism leading to such a distribution. Herein, we demonstrate that a preferential deposition of Pt on WO_3 occurs and provide experimental data to explain the mechanism which induces this phenomenon.

For the synthesis of WO_3 particles with well-structured facets, methods for crystal-facet engineering are very suitable.[10] By using hydrothermal synthesis, researchers have been able to obtain WO_3 with well-defined morphologies, such as nanorods,[11] nanowires,[12] nanoplates/nanosheets,[13] nanourchins,[12b,14] and flowerlike morphologies.[15] We synthesized well-defined platelike WO_3 on the basis of a method described by Su et al.[13a] Platinum was photodeposited by a similar method described by Purwanto et al. by the use of the precursor $[H_2PtCl_6]\cdot 6H_2O$ at pH 3, 4, and 6.[8c] We also applied the impregnation of Pt on our samples by using a method proposed by Yoshimura et al.[16] Finally, we performed aqueous-phase AFM studies to determine whether different crystal facets of WO_3 possess (pH-dependent) opposite intrinsic surface charges.

By using the method of Su et al.,[13a] we obtained platelike WO_3 particles of the monoclinic phase with well-defined facets and a specific BET surface area of approximately $8.4\ m^2 g^{-1}$. After the photodeposition of Pt on such WO_3 particles, we analyzed the resulting particles by high-resolution TEM (HRTEM), X-ray photoelectron spectroscopy (XPS), and inductively coupled plasma atomic emission

[*] K. Wenderich, Prof. G. Mul
Photocatalytic Synthesis Group
MESA+ Institute for Nanotechnology, University of Twente
P.O. Box 217, 7500 AE Enschede (The Netherlands)
E-mail: g.mul@utwente.nl
A. Klaassen, Dr. I. Siretanu, Prof. F. Mugele
Physics of Complex Fluids Group
MESA+ Institute for Nanotechnology, University of Twente

[**] This project is funded by the Dutch National Research School Combination Catalysis Controlled by Chemical Design (NRSC-Catalysis). We thank the following people for their help: Mark Smithers for performing HRSEM measurements, Enrico Keim for HRTEM measurements, and Gerard Kip for XPS measurements. We are also grateful to Boudewijn de Smeth from the GeoScience Laboratory (ITC faculty, University of Twente) for performing ICP-AES measurements.

Supporting information for this article is available on the WWW under http://dx.doi.org/10.1002/anie.201405274.

spectroscopy (ICP-AES) to identify the Pt particle size and loading (see Figure S1 in the Supporting Information for an HRTEM image of the Pt particles). Energy-dispersive X-ray spectroscopy (EDX) confirms that the particles consist of Pt. On the basis of the electron microscopy data, we determined that the Pt particles have a diameter in the range of approximately 5–10 nm. Additionally, the XPS data revealed that the percentage of Pt atoms on the surface of Pt/WO_3 obtained through photodeposition was 1.5 atom%, whereas the percentage of surface Pt atoms in Pt/WO_3 obtained through impregnation was 2.9 atom% (see Figure S2 and Table S1 in the Supporting Information). ICP-AES measurements show that the Pt loading obtained through photodeposition is 0.8 wt%. When impregnation was used, the Pt loading was 1.8 wt%. Furthermore, XPS analysis showed that potential contamination by chlorine or carbon atoms as a result of the WO_3 synthesis was absent.

Figure 1 shows high-resolution SEM images of platinum-loaded platelike WO_3 prepared by photodeposition in a procedure based on the use of $[H_2PtCl_6]\cdot 6H_2O$. We observe two phenomena. First, a preferred positioning of Pt particles

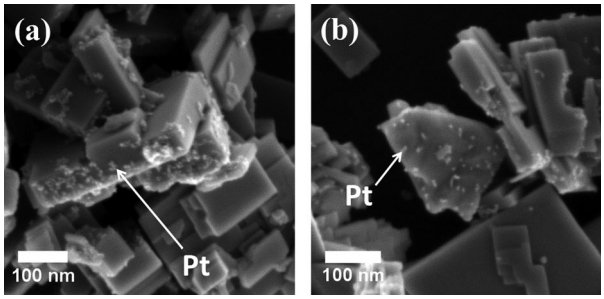

Figure 1. HRSEM images of as-synthesized platelike WO_3 loaded with Pt particles through photodeposition with $[H_2PtCl_6]\cdot 6H_2O$ as the precursor. a) Positioning of the Pt particles seems to take place at the edges/smaller facets. b) Some WO_3 particles lose their well-defined morphology by photodeposition.

occurs for well-defined crystals of WO_3 at the smaller facets. Often the dominant facet of the platelike morphology is void of any Pt particles. Statistically, we determined the ratio of Pt particles on the edges/small facets to those on the dominant facets to be 5:1 (see Tables S2 and S3). In these crystals, we determined the dominant facet to be the (002) facet and the edged facet to be (020), as confirmed by HRTEM and AFM studies (see Figure S3). Second, we observe in the HRSEM images that some crystals have lost their well-defined morphology after the photodeposition procedure. A clear preference of Pt for specific facets is not so evident in these domains of the sample. We hypothesize that during the photodeposition of Pt on WO_3, a (local) increase in the pH value occurs, possibly induced by platinum-related photocatalytic hydrogen formation, and results in instability of the WO_3 crystals in solution. (Photo)corrosion of WO_3 is known to be significant at $pH > 4$. Indeed, when the photodeposition reaction was performed at pH 6, a significantly more dramatic restructuring of WO_3 was apparent (Figure 2), and the phenomenon of preferred deposition was no longer observed.

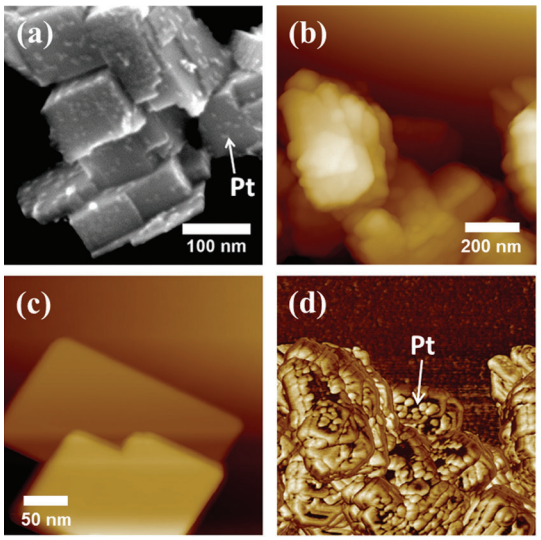

Figure 2. a) HRSEM image of as-synthesized platelike WO_3 loaded with Pt particles through photodeposition with $[H_2PtCl_6]\cdot 6H_2O$ as the precursor at pH 6. b) AFM height and d) AFM phase images (obtained in tapping mode) of WO_3 loaded with Pt particles. c) AFM height image (obtained in tapping mode) of as-synthesized platelike WO_3 particles deposited on a silicon substrate. The positioning of the Pt particles is no longer visible.

HRSEM and AFM topography images shown in Figure 2 and Figure S4 (see the Supporting Information) clearly illustrate that WO_3 particles after photodeposition had lost their well-defined initial platelike structure (Figure 2c) and had a rougher, rounder morphology. It is difficult to distinguish the difference between the dominant facet and edges.

Interestingly, HRSEM images of platinum-loaded platelike WO_3 obtained through impregnation with the same precursor ($[H_2PtCl_6]\cdot 6H_2O$) show similar phenomena (Figure 3). Preferred Pt deposition on the subordinate facets is observed, again with a statistical ratio of Pt particles on the edges/small facets to those on the dominant facets of 5:1 (see Table S4). This result also suggests that the size and distribution of the Pt particles do not change significantly as a consequence of the somewhat higher loading of the impregnated sample. Still, at significantly higher loading the

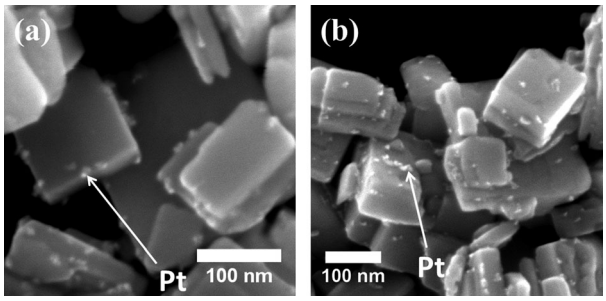

Figure 3. HRSEM images of as-synthesized platelike WO_3 loaded with Pt particles through impregnation with $[H_2PtCl_6]\cdot 6H_2O$ as the precursor. a) Again, positioning of the Pt particles seems to take place at the edges. b) Some WO_3 particles have changed morphology after impregnation. Structure-directed deposition is no longer obvious in these domains.

geometrical particle distribution might be different; this possibility will be the subject of a future study. Although to a lesser extent, some corrosion of WO_3 also occurred in the impregnation procedure, thus leading to domains where Pt deposition was more arbitrary. We hypothesize that this behavior is again caused by an increase in the pH value, induced in this procedure by the decreasing HCl concentration during the water-evaporation step at 100 °C.

Attempts to use the cation $[Pt(NH_3)_4]^{2+}$ rather than the anion $[PtCl_6]^{2-}$ to create Pt nanoparticles on WO_3 crystals by photodeposition were unsuccessful: No Pt particles were observed in SEM images, in agreement with previously reported studies.[17] Interestingly, impregnation with this precursor appears to yield a significant fraction of Pt particles on the dominant facets of the platelike WO_3 (Figure 4). Notably, the Pt particles are also considerably larger than those formed with $[H_2PtCl_6]\cdot 6H_2O$ (Figure 1), ranging from

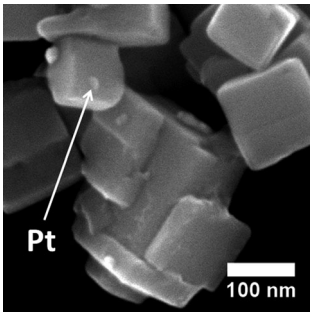

Figure 4. HRSEM image of as-synthesized platelike WO_3 loaded with Pt particles through impregnation with $[Pt(NH_3)_4(NO_3)_2]$ as the precursor. No obvious preferred positioning of the Pt particles is observed, with several Pt particles present on the dominant facets. The Pt particles also appear larger than when $[H_2PtCl_6]\cdot 6H_2O$ was used as the precursor.

10 to 25 nm in diameter. This difference in particle size is in agreement with earlier studies by Ma et al.[18]

The results strongly suggest that the structure-directed (photo)deposition of Pt on monoclinic WO_3 is adsorption-induced. To determine whether an intrinsic surface charge is present for WO_3 crystals, AFM studies were conducted in water (pH 3 or pH 6, 10 mM NaCl) with a sharp negatively charged oxidized Si tip (Figure 5). At a pH value of around 6, the weakly repulsive force recorded on the basal planes indicates a weak negative surface charge. The absolute value amounts to 10–20% of the much more repulsive adjacent silica substrate. The charge density of the latter is approximately $-0.5\ C\,m^{-2}$ under the conditions of the present experiments.[19] The negative charge is in agreement with the macroscopic observation of Kim et al., who showed a negative surface charge of WO_3 by ζ-potential measurements.[6a] However, the results suggest a different, in the present case slightly positive surface charge along the edges of the WO_3 crystals.

Similar behavior was observed at a pH value of about 3, at which the interaction force between the tip and the basal

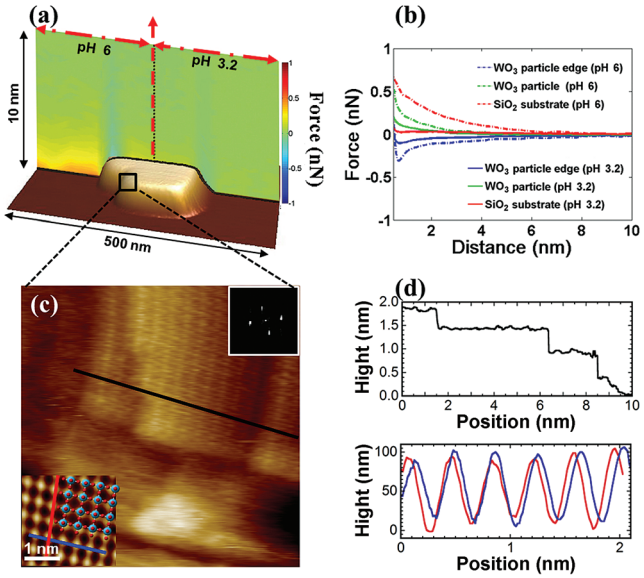

Figure 5. a) Combined 2D force field obtained by measuring 55 single force-versus-distance curves along a line in the *x* direction over a silicon oxide/WO_3 sample in 10 mM aqueous NaCl at pH 3.2 and 6. b) Averaged force curves from measurement in (a) plotted versus tip–sample distance. At pH 6, a mild repulsive force represents a mild negative surface charge of facets of the WO_3 particle (green), whereas an attractive force represents a positive surface charge (blue). The WO_3 particle was deposited on silica as a support, which was significantly negatively charged (red). At pH 3.2, the interaction force between the tip and the basal planes of the WO_3 particle is more repulsive. c) High-resolution noncontact amplitude-modulated AFM topographic images of the WO_3 surface taken in 10 mM aqueous NaCl. The top inset shows a two-dimensional fast Fourier transformation pattern of height images. The bottom inset shows the zoom of an atomic-scale image on basal planes ((002) facet) after processing with a Fourier transformation superimposed with an X-ray crystal structure in the *ab* plane. Protrusions arranged in a quasisquare structure agree well with the theoretical X-ray crystal structure and the arrangement of tungsten atoms. d) Top: Height profile taken along the black line in (c) shows the atomic steps. Bottom: Height profiles in the red and blue directions shown in the bottom inset of (c). The height profiles in the red and blue directions display periodicities of approximately 0.38 nm.

planes of a WO_3 particle were more repulsive as compared to silica. As the pH value of about 3 is very close to the isoelectric point (IEP) of silica ($IEP_{SiO_2} \approx 3$) rather than WO_3 ($IEP_{WO_3} \approx 2$), the surface is still negatively charged,[6a] in agreement with the observed location of the Pt nanoparticles prepared by using solutions of $[PtCl_6]^{2-}$: Since the edges appear positively charged, sorption of the negatively charged $[PtCl_6]^{2-}$ is probably preferred at these locations.

To understand what causes the clear preference of Pt for sorption on specific facets, we proceeded to image the WO_3-particle surface at atomic resolution. Figure 5c shows the amplitude-modulated height image of a WO_3 particle equilibrated in 10 mM aqueous NaCl at atomic resolution. The image was obtained with a super-sharp tip at room temperature. It was recorded along the WO_3 particle, so that the basal plane and edges can be observed at the same time. The top right corner, which corresponds to the basal plane of the particle, reveals the monoclinic symmetry caused by the arrangement of the protrusions in a quasisquare structure

with spacings of approximately 0.38 nm in the *a* and *b* directions, consistent with the crystallographic data (as emphasized in the inset in the bottom left corner). In analogy with earlier observations for gibbsite platelets,[20] closer to the edge a higher density of atomic steps (black line in Figure 5c,d), a distorted lattice, and the presence of various structural defects were observed. These features could explain the preponderant heterogeneous electrostatic interactions and charge properties, which probably contribute to the observed (positive) charges and preferential $[PtCl_6]^{2-}$ adsorption at these locations (see Figure S3 for more details).

We speculate that similar, positively charged structural defects might be formed upon (photo)corrosion of the dominant facet of WO_3 under mildly basic conditions. $[PtCl_6]^{2-}$ ions adsorb on these newly formed sites, thus explaining the presence of some particles on the dominant facets. When more drastic (photo)corrosion takes place (Figure 2), the vast restructuring of the crystal leads to an arbitrary deposition of Pt, which most likely has a more complicated origin than simple electrostatic interactions. More detailed and extensive AFM studies at different stages of corrosion are required to investigate how structural defects are formed, and to clarify the mechanism of platinum-particle formation on such severely corroded crystals.

In summary, facet-preferred (photo)deposition of Pt on WO_3 was observed, and was predominantly determined by differences in intrinsic surface charge. Prior to photoreduction and/or thermal decomposition, $[PtCl_6]^{2-}$ ions adsorbed preferentially on positively charged surfaces, thus leading to the observed specific geometrical distribution. The AFM results are in agreement with sorption-induced geometrical particle distributions.[2] We propose that light-induced preferential migration of electrons and holes to specific crystal facets is a less valid hypothesis to explain the observed particle distributions.[1,3,4]

Further research is under way to verify whether the facet-preferred deposition of metals or metal oxides is consistently driven by intrinsic differences in surface charge. Second, we aim to verify if the presence of Pt in a specific, but different geometrical distribution is of relevance for photocatalytic activity. In this case, an increase in the pH value should be prevented at all times, to prevent loss of integrity of the well-defined crystals of WO_3 or other semiconductor oxides, and thus loss of the preferred spatial distribution of Pt deposition.

Received: May 14, 2014
Revised: June 20, 2014
Published online: July 23, 2014

Keywords: atomic force microscopy · crystals · electron microscopy · nanomaterials · photocatalysis

[1] T. Ohno, K. Sarukawa, M. Matsumura, *New J. Chem.* **2002**, *26*, 1167 – 1170.
[2] Y. Miseki, H. Kato, A. Kudo, *Energy Environ. Sci.* **2009**, *2*, 306 – 314.
[3] K. Iizuka, T. Wato, Y. Miseki, K. Saito, A. Kudo, *J. Am. Chem. Soc.* **2011**, *133*, 20863 – 20868.
[4] R. Li, F. Zhang, D. Wang, J. Yang, M. Li, J. Zhu, X. Zhou, H. Han, C. Li, *Nat. Commun.* **2013**, *4*, 1432.
[5] H. Zheng, J. Z. Ou, M. S. Strano, R. B. Kaner, A. Mitchell, K. Kalantar-Zadeh, *Adv. Funct. Mater.* **2011**, *21*, 2175 – 2196.
[6] a) J. Kim, C. W. Lee, W. Choi, *Environ. Sci. Technol.* **2010**, *44*, 6849 – 6854; b) A. Kudo, Y. Miseki, *Chem. Soc. Rev.* **2009**, *38*, 253 – 278.
[7] a) S. H. S. Chan, T. Y. Wu, J. C. Juan, C. Y. Teh, *J. Chem. Technol. Biotechnol.* **2011**, *86*, 1130 – 1158; b) R. Abe, M. Higashi, K. Domen, *ChemSusChem* **2011**, *4*, 228 – 237.
[8] a) R. Abe, H. Takami, N. Murakami, B. Ohtani, *J. Am. Chem. Soc.* **2008**, *130*, 7780 – 7781; b) U. A. Joshi, J. R. Darwent, H. H. P. Yiu, M. J. Rosseinsky, *J. Chem. Technol. Biotechnol.* **2011**, *86*, 1018 – 1023; c) A. Purwanto, H. Widiyandari, T. Ogi, K. Okuyama, *Catal. Commun.* **2011**, *12*, 525 – 529; d) M. K. Aminian, J. Ye, *J. Mater. Res.* **2010**, *25*, 141 – 148.
[9] a) M. Qamar, Z. H. Yamani, M. A. Gondal, K. Alhooshani, *Solid State Sci.* **2011**, *13*, 1748 – 1754; b) Z. Xu, I. Tabata, K. Hirogaki, K. Hisada, T. Wang, S. Wang, T. Hori, *Mater. Lett.* **2011**, *65*, 1252 – 1256.
[10] G. Liu, J. C. Yu, G. Q. Lu, H. M. Cheng, *Chem. Commun.* **2011**, *47*, 6763 – 6783.
[11] a) J. Zhu, S. Wang, S. Xie, H. Li, *Chem. Commun.* **2011**, *47*, 4403 – 4405; b) J. Wang, E. Khoo, P. S. Lee, J. Ma, *J. Phys. Chem. C* **2008**, *112*, 14306 – 14312; c) R. F. Mo, G. Q. Jin, X. Y. Guo, *Mater. Lett.* **2007**, *61*, 3787 – 3790.
[12] a) Z. Gu, H. Li, T. Zhai, W. Yang, Y. Xia, Y. Ma, J. Yao, *J. Solid State Chem.* **2007**, *180*, 98 – 105; b) Z. Gu, T. Zhai, B. Gao, X. Sheng, Y. Wang, H. Fu, Y. Ma, J. Yao, *J. Phys. Chem. B* **2006**, *110*, 23829 – 23836.
[13] a) X. Su, F. Xiao, Y. Li, J. Jian, Q. Sun, J. Wang, *Mater. Lett.* **2010**, *64*, 1232 – 1234; b) J. Wang, P. S. Lee, J. Ma, *J. Cryst. Growth* **2009**, *311*, 316 – 319.
[14] S. Jeon, K. Yong, *J. Mater. Chem.* **2010**, *20*, 10146 – 10151.
[15] a) Y. Zhao, H. Chen, X. Wang, J. He, Y. Yu, H. He, *Anal. Chim. Acta* **2010**, *675*, 36 – 41; b) J. Yu, L. Qi, *J. Hazard. Mater.* **2009**, *169*, 221 – 227.
[16] K. Yoshimura, T. Hakoda, S. Yamamoto, M. Yoshikawa, *J. Phys. Chem. Solids* **2012**, *73*, 696 – 698.
[17] C. R. K. Rao, D. C. Trivedi, *Coord. Chem. Rev.* **2005**, *249*, 613 – 631.
[18] S. S. K. Ma, K. Maeda, R. Abe, K. Domen, *Energy Environ. Sci.* **2012**, *5*, 8390 – 8397.
[19] D. Ebeling, D. van den Ende, F. Mugele, *Nanotechnology* **2011**, *22*, 305706.
[20] I. Siretanu, D. Ebeling, M. Andersson, S. Stipp, A. Philipse, M. Stuart, D. van den Ende, F. Mugele, *Sci. Rep.* **2014**, *4*, 4956.

